An Experimental and Numerical Investigation Into the Mechanisms of Rotating Instability

Joachim März
Mem. ASME
STN Atlas Elektronik GmbH,
Bremen 28305, Germany

Chunill Hah
Fellow ASME
NASA Glenn Research Center,
Cleveland, OH 44135
e-mail: chunhill.hah@grc.nasa.gov

Wolfgang Neise
Mem. ASME
DLR, Institute of Propulsion
Technology,
Berlin, Germany

This paper reports on an experimental and numerical investigation aimed at understanding the mechanisms of rotating instabilities in a low speed axial flow compressor. The phenomena of rotating instabilities in the current compressor were first identified with an experimental study. Then, an unsteady numerical method was applied to confirm the phenomena and to interrogate the physical mechanisms behind them. The experimental study was conducted with high-resolution pressure measurements at different clearances, employing a double phase-averaging technique. The numerical investigation was performed with an unsteady 3-D Navier-Stokes method that solves for the entire blade row. The current study reveals that a vortex structure forms near the leading edge plane. This vortex is the result of interactions among the classical tip-clearance flow, axially reversed endwall flow, and the incoming flow. The vortex travels from the suction side to the pressure side of the passage at roughly half of the rotor speed. The formation and movement of this vortex seem to be the main causes of unsteadiness when rotating instability develops. Due to the nature of this vortex, the classical tip clearance flow does not spill over into the following blade passage. This behavior of the tip clearance flow is why the compressor operates in a stable mode even with the rotating instability, unlike traditional rotating stall phenomena. [DOI: 10.1115/1.1460915]

Introduction

Rotating instability is a phenomenon that occurs in the tip flow region of axial compressor stages during stable operation. It can be observed in highly staggered rotors with significant tip clearance and is strongest at high-load operating points where the characteristic levels off.

In this condition, the single-stage fan under investigation radiates an audible, whistling tone, and wall pressure spectra in the vicinity of the rotor disk exhibit nonrotational components. These form a characteristic hump at roughly half of the blade passing frequency (BPF), as can be seen in Fig. 1.

Previous work on the axial fan test stand at DLR Berlin focused on the effects of varying tip clearance and blade number on rotating instability. Circumferential mode analysis was performed and led to the model of a rotating source mechanism that moves relative to the blade row at a fraction of the shaft speed, not unlike rotating stall cells but with higher mode orders (Kameier and Neise [1], Liu et al. [2], März et al. [3]).

Spectra similar to those seen in Fig. 1 were encountered in pressure measurements in the first stage of an axial multistage compressor, as reported by Baumgartner et al. [4]. Structural vibrations excited by this non-rotational source added to the relevance of the phenomenon.

The effect could also be reproduced in the third stage of the low-speed research compressor at TU Dresden after enlarging the stage's tip clearance sufficiently (Müller and Mailach [5]).

Experimental Study

Test Facility and Instrumentation. The present investigation was performed on the axial fan test stand of DLR Berlin. This rig is a low-speed single-stage fan with outlet guide vanes. Its design parameters are given in Table 1. The tip clearance can be varied by exchanging casing segments with the impeller diameter remaining constant. Fan characteristics at different tip clearances are shown in Fig. 2. Characteristics were recorded by closing and opening the throttle and thus exhibit hysteresis in the stalled region.

An access window incorporating 40 piezo-resistive pressure sensors was installed. The sensors were spaced as closely as possible to provide adequate resolution of the pressure field in the region of interest. Transducers needed to be staggered to achieve an axial resolution of 1.33 mm (see Fig. 3). In addition, a pressure sensor was installed on the blade tip suction side at 36% chord and 3 mm inwards from the blade tip.

Frequency response of the amplifier/transducer/tap combination was verified and found to be within 3 dB up to 17 kHz bandwidth with a linear phase relationship. To correct for transducer drift, the dc component of the signals was corrected against a row of 20 static pressure taps. These were periodically sampled with a scanivalve during measurements. Trigger pulses for ensemble averaging were derived from a shaft encoder.

Together with rotor position/operating point signals, 48 channels were acquired at 51.2 kSamples/s. At a suitably chosen rotor speed of 2560/min, this sample rate results in a resolution of 40×50 (axial $\times$ circumferential) pressure samples per blade passage.

Data acquisition was performed using a VXI front-end, sampling 60 seconds of time data at 16-bit resolution onto throughput disks. The resulting 590 megabytes per operating point configuration could be stored on one CDROM each.

Measured Flow Characteristics of Rotating Instability. The current compressor was investigated extensively to identify rotating instability along the fan operating lines with four different clearance gaps. The rotating instability was most clearly observed near the maximum fan loading at the two largest tip gaps of 2.8 and 5.6% of tip axial chord. In the following sections, overall

Contributed by the International Gas Turbine Institute and presented at the International Gas Turbine and Aeroengine Congress and Exhibition, New Orleans, Louisiana, June 4–7, 2001. Manuscript received by the IGTI, February 12, 2001; revised Manuscript received November 7, 2001. Paper No. 2001-GT-536. Review Chair: R. A. Natole.

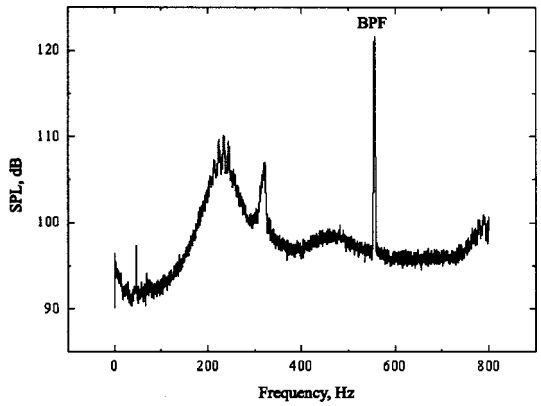

Fig. 1 Wall pressure spectrum with rotating instability components $n=1400$/min, BPF=560 Hz

Table 1 Axial fan test stand

rotor blade #	24
stator blade #	17
stator airfoil	flat circular arc
rotor diameter	452.4 mm
tip clearance	0.3, 0.6, 1.2 or 2.4 mm (ζ=0.7, 1.4, 2.8, 5.6 percent of tip chord)
design point	3000/min, ϕ=0.230
hub-to-tip ratio	0.62
tip stagger angle	27°

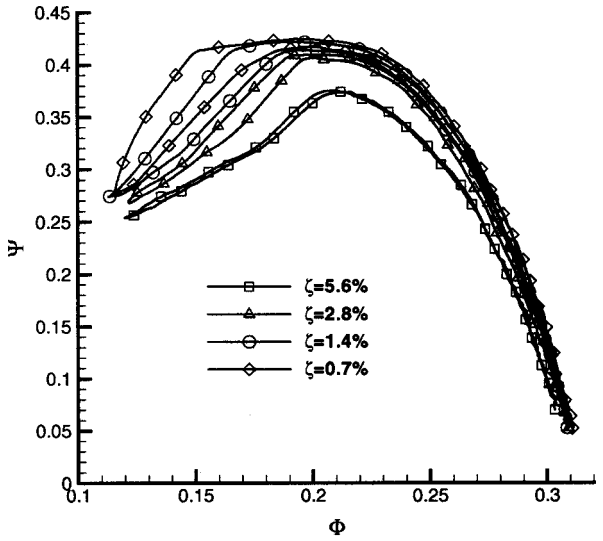

Fig. 2 Fan characteristics at different tip clearances

observations will be presented first. More detailed flow features for the 2.8% tip clearance case near maximum loading will then be shown, since this case was also analyzed numerically to study the flow mechanisms.

Pseudo-Spatial Correlation. A line of sensors located across the rotor disk and sampled simultaneously delivers instantaneous scan lines of the wall pressure field. The rotor's motion results in a sweep across subsequent passages. Thus, with a sufficient sampling rate, a highly resolved picture of the pressure field can be

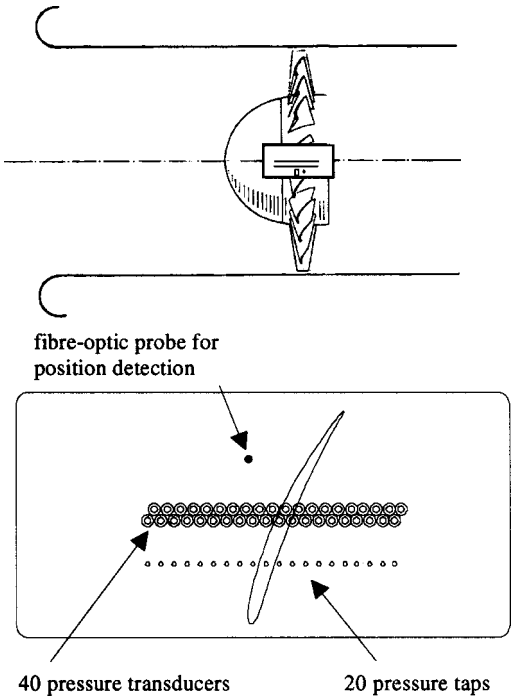

Fig. 3 Position and layout of the access window

obtained by mapping pressure time histories onto the rotor circumference. This "pseudo-spatial correlation" is done under the assumption that the pressure field is steady in the relative frame.

Unsteadiness in the relative frame will result in an aliasing phenomenon. The spatial correlation between neighboring scan lines breaks up when the relative frame pressure field is unsteady on a time scale comparable to 1/BPF. Thus, once the flow becomes unsteady in the relative frame, this technique will only show a convolution of the unsteady pressure field with the blade passing frequency.

Figure 4 shows time-lapse plots for four different tip clearances, with operating points suitably chosen to show rotating instability in the latter two cases. Steady flow dominates the endwall region in the cases with tip clearances of $\zeta=0.7$ and 1.4%. In addition to the potential flow field, the roll-up and trajectory of the tip clearance vortex can clearly be seen. Some disturbances are introduced by the blade wake and in the area between the blade and the departing tip clearance vortex.

At tip clearances of $\zeta=2.8$ and 5.6%, highly unsteady flow takes over. The potential flow field varies in its intensity from blade to blade. While, for the aforementioned reasons, these structures cannot be interpreted as an instantaneous spatial pattern, the presence of a rather localized low-pressure spot can be noticed at seemingly random positions in the rotor entry plane. Instantaneous pressure values at the spot's location go down to $C_p=-3$.

Ensemble Averaging. Ensemble averaging overcomes the aliasing problem by eliminating any non-rotational components in the pressure signals. The ensemble-averaged contour plots look very similar to the steady flow patterns at smaller tip clearance, but detail is reduced considerably. In Fig. 5, a blade-to-blade average is taken over 150 samplings of one blade passage using a trigger signal from the shaft encoder.

Standard Deviation. As a by-product of ensemble averaging, the standard deviation can be plotted as a measure of the "local unsteadiness" in the passage. Standard deviation is computed here as

$$p'_{\mathrm{rms}}=\sqrt{\overline{(p_{ij}-\mu_{ij})^2}}$$

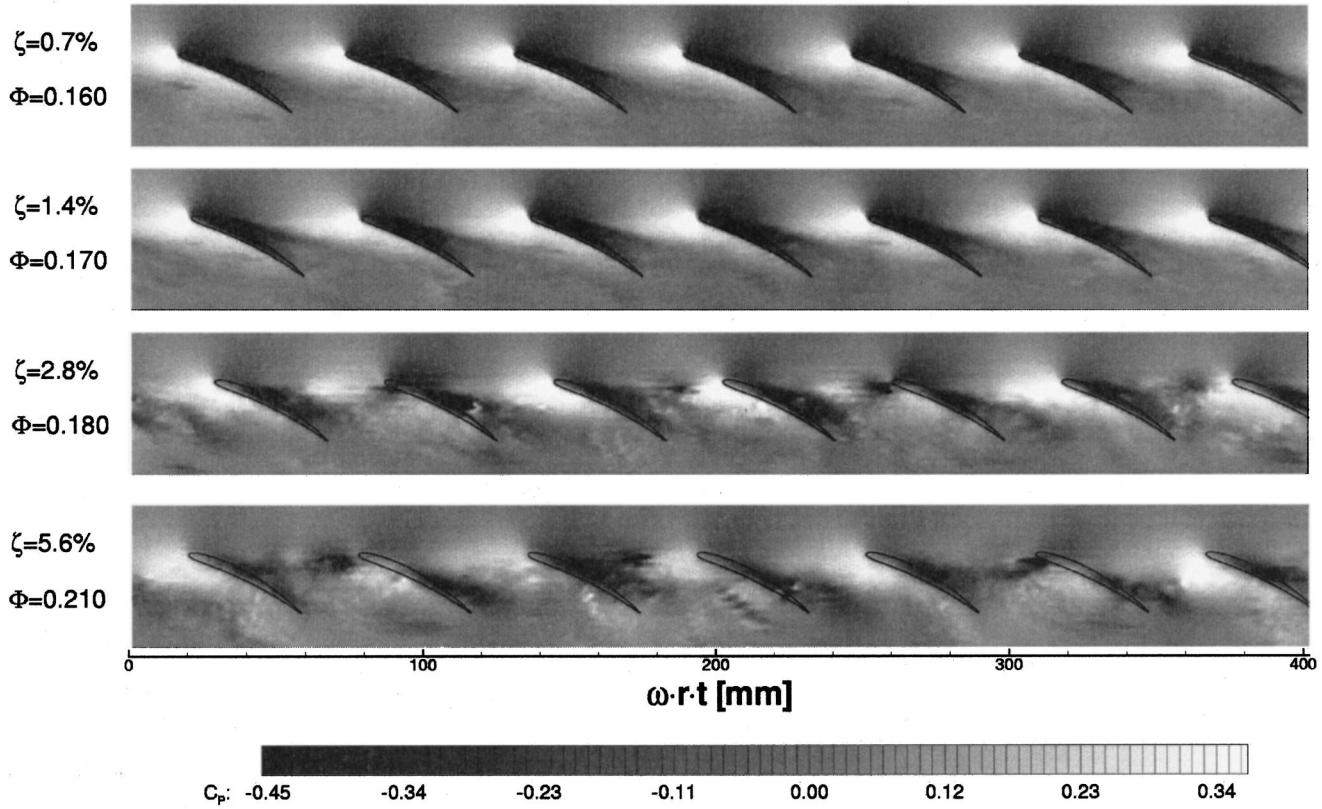

Fig. 4 Time-lapse plots of casing wall pressure at different tip clearances

with the instantaneous pressure value p_{ij} and the ensemble-averaged pressure μ_{ij} at location (i,j) within the passage. While not an immediate physical quantity, it maps the locus of unsteadiness in the passage.

Unfortunately, a ± 0.5 sample uncertainty in acquiring the trigger pulse lets steep gradients in the pressure field appear as fluctuations. High values of p'_{rms} underneath the airfoil/tip gap position as shown in Fig. 5 must be attributed to this effect.

It can be seen that there is a high fluctuation content in the entry plane of the rotor. In particular, maximum fluctuation amplitude can be found just ahead of the blade leading edge, stretching to the neighboring blade's suction side.

At the near maximum loading conditions with the two large clearances shown in Fig. 4, the phenomena of rotating instability were identified with the whistling tone from the compressor and also through pressure spectra. For the current study, the third case with the nominal tip gap of 2.8% at the flow coefficient of 0.18 is investigated in detail. The measurements correspond to the upper branch of the characteristic in Fig. 2.

Double Phase Averaging. To gain a closer physical understanding of the mechanism of this unsteadiness, it would be necessary to ''de-convolute'' the pressure time traces and ''transform'' them into the relative frame in order to see the unsteady process as does an observer in the relative frame.

After more closely examining the blade sensor signal in the presence of rotating instability, a double phase averaging algorithm was developed allowing display of the rotating instability cycle as an animation virtually in the relative frame.

It turns out that the blade sensor signal has a strong periodic content (see Fig. 6). Such a period can be regarded as one ''cycle'' of rotating instability.

To assemble an animation of this cycle, pressure samples must be collected

(a) for all locations in the blade passage (axial and circumferential),
(b) for all phase bins within one period of the blade pressure signal.

The wall pressure signals are only correlated to the blade sensor signal when the instrumented blade passes underneath the access window. These ''position coincidences'' are collected, evaluated by phase, and then re-sorted into phase bins (see Fig. 7). Thus, the double phase averaging now consists of averaging stripes of equal phase and circumferential position, i.e. belonging to the same ''bin.'' In this way, 60 s of data were split into ''position coincidences,'' assigned a phase value, and averaged, yielding about 70 averages per 10 deg phase bin. This procedure is based on two assumptions:

(a) The observed phenomenon must not have a circumferential preference; i.e., it must rotate freely in the rotor and must not be bound to some upstream disturbance such as stators or other inlet distortions.
(b) The observed phenomenon is correlated over some extent in the circumferential direction, at least over the width of the data window being averaged.

Figure 8 shows pressure contours in the relative frame during one period of rotating instability. Apart from substantial fluctuations in the potential flow field, the most prominent feature is a low-pressure spot that travels continuously from the middle blade's suction side to the following blade's pressure side. This low-pressure spot is interpreted as the footprint of a radial vortex. It is created much like a starting/unstarting vortex from the airfoil, travels across the blade passage, and interacts with the following blade, giving rise to a new ''starting vortex.'' However, in order to

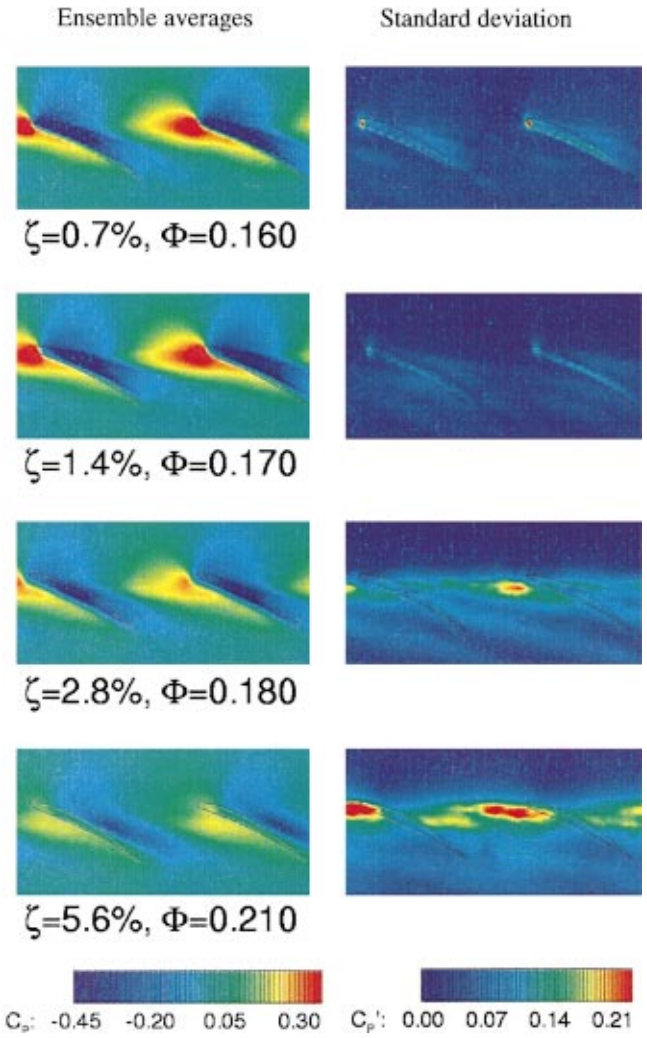

Fig. 5 Ensemble averages and standard deviation plots for varying tip clearance and selected operating points

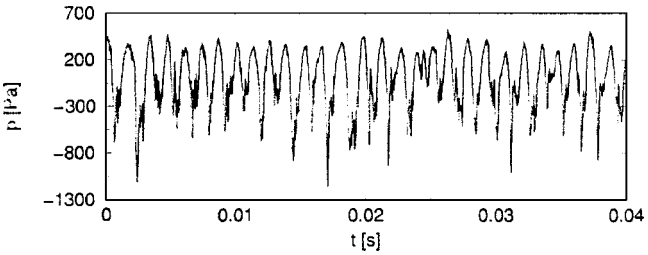

Fig. 6 Time history of blade pressure signal

fully understand this unsteady endwall flow, knowledge of flow quantities in the deeper layers of the endwall flow would be required.

Numerical Study

The experimental study presented in the previous section provides evidence of rotating instabilities and a description of the unsteady behavior through measurements and analysis of casing and blade tip pressures. A numerical investigation was performed to examine detailed flow structures so that the physical mechanisms behind the unsteady phenomena could be adequately explained. The rotor with a tip gap of 2.8% and a flow coefficient of 0.18 was numerically analyzed.

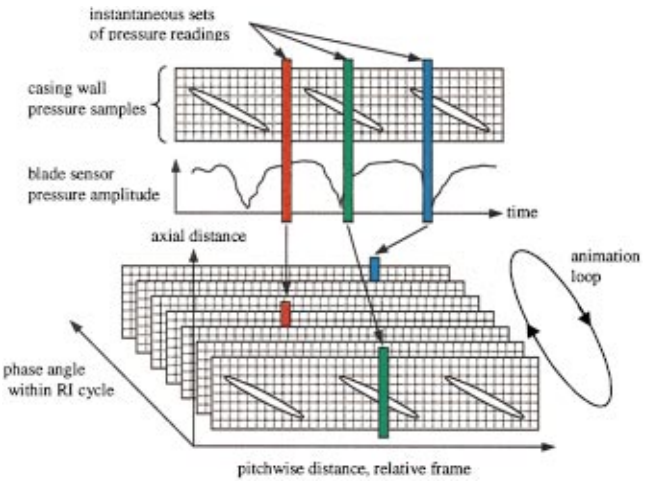

Fig. 7 Sorting algorithm for double phase averaging

Numerical Method. A three-dimensional steady Navier-Stokes code that has been successfully tested for a wide range of turbomachinery flows (Hah [6,7]) was modified to execute a time-accurate simulation of the full annulus of the compressor. The downstream stator was not included in the numerical analysis since the measurements showed that the influence of the stator on the rotating instability was negligible. At each time step, the governing equations are solved with an implicit relaxation method using a fully conservative control volume approach. Previous studies (Cho et al. [8], Hah et al. [9]) have shown that high-order discretization schemes are necessary in both space and time to avoid excessive numerical dissipation. A third-order accurate interpolation scheme is used for the spatial discretization of the convection terms, and central differencing is used for the diffusion terms. The method is of second-order spatial accuracy with smoothly varying grids. For the time-dependent terms, an implicit second-order scheme is used. For unsteady flow calculations, the size of the time step is primarily determined by the requirement for physical accuracy. However, the time step is also restricted by numerical stability. For the current implicit time integration approach, a subiteration is performed at each time step. Residuals of each finite difference equation are integrated over the entire flow domain at each sub-iteration. When the integrated residuals of all the equations are reduced by four orders of magnitude from their initial values during the subiteration, the solution is advanced to the next time step. A modified two-equation model is used to estimate Reynolds stresses. The turbulence model applies either a wall function or a low-Reynolds-number correction near the wall depending on the flow and grid resolution near the wall.

At the inlet of the computational domain, the total pressure, total temperature, and two velocity components are specified. Since no unsteady measurements of static pressure or other flow variables were available downstream of the rotor, circumferentially averaged static pressure was specified on the shroud at the outlet of the computational domain. Nonreflective procedures are used at the exit to minimize the influence of upstream effects. Further details of the computational procedures for the unsteady flow analysis are given by Hah et al. [9, 10].

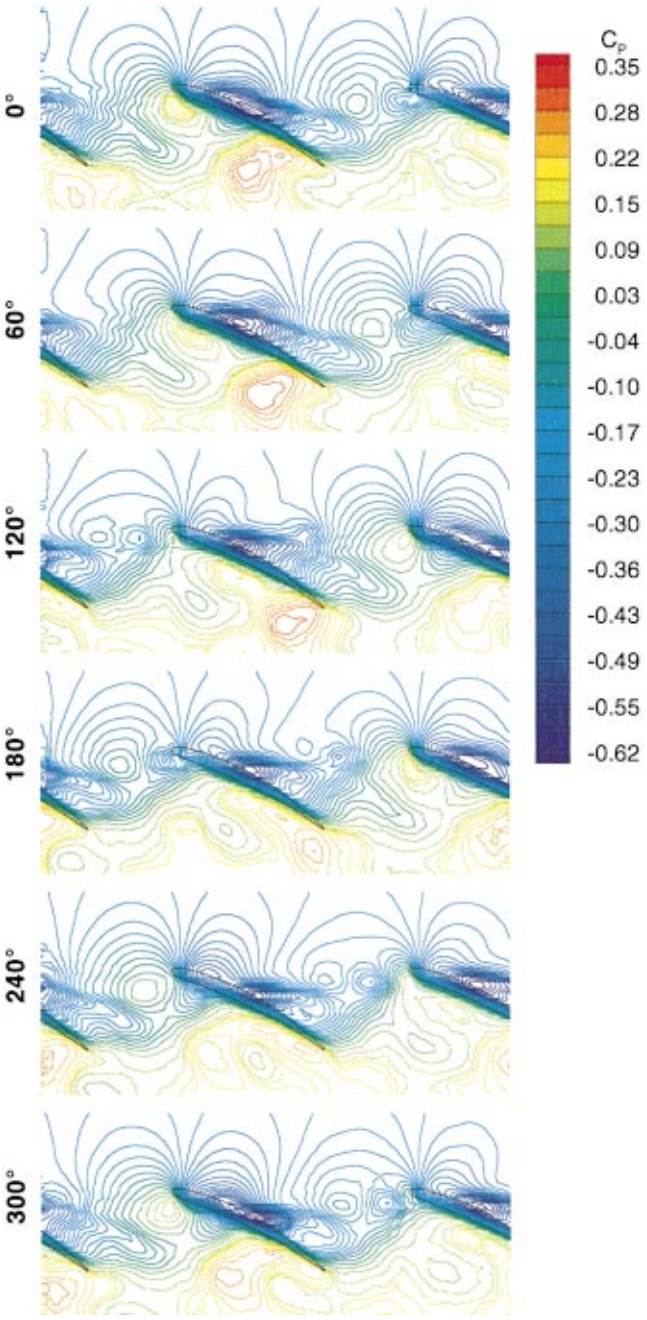

Fig. 8 Relative frame pressure field during one cycle of rotating instability

The rotor consists of 24 blades. To minimize the computational resources required, a coarse grid consisting of 40 nodes in the blade-to-blade direction, 36 nodes in the spanwise direction, and 102 nodes in the streamwise direction was used for each blade passage in the unsteady full-annulus simulation. Four spanwise grid nodes describe the tip clearance. The grid contains a total of 3.5 million nodes.

Because the total number of grid points was restricted to achieve a practical computational turn-around time, the grid was clustered near the tip region. The current grid resolves the main flow feature, namely the interaction between the tip clearance flow and the incoming flow in a low-speed regime, reasonably well. The calculation was executed on a CRAY C-90 computer, requiring roughly ten single-CPU hours to advance the time-accurate solution by one blade pitch revolution on the current computational grid.

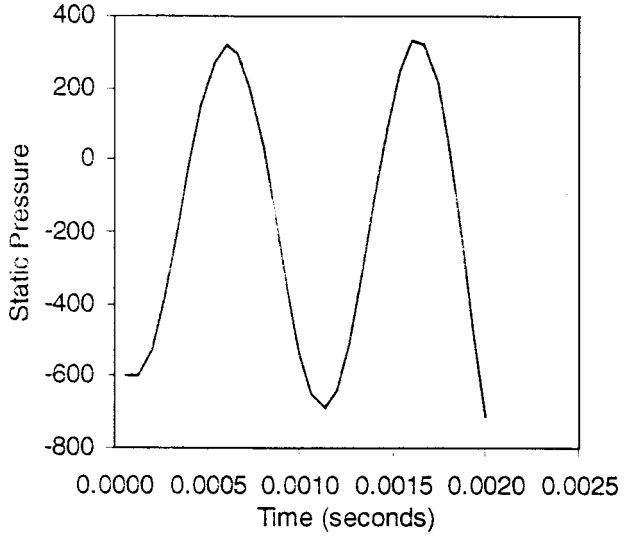

Fig. 9 Calculated time history of blade pressure

Calculated Characteristics of Rotating Instability. To obtain an initial flow field for the unsteady full-annulus calculation, a steady single-passage calculation was first performed. However, the steady calculation does not provide converged solutions below a flow coefficient of 0.2. Therefore, the steady single-passage solution at a flow coefficient of 0.2 was used as an initial solution for the unsteady full-annulus calculation. The rotor exit pressure at the casing was then gradually raised by an increment of 0.001 psi to obtain a flow rate of 0.18.

The unsteady full-annulus calculated flow field becomes unsteady at mass flow rates below 0.2. The unsteadiness is mainly due to unsteady movement of the tip clearance vortex, which is amplified by an increase in the tip gap. Unsteady wandering of the tip clearance vortex for relatively large tip gaps was also observed by Zierke et al. [11].

At the flow rate of 0.18, a rotating instability was observed in the numerical solution. After about two rotor revolutions, an almost periodic unsteady solution was observed. The fan characteristics in Fig. 2 show hysteretic behavior for the two largest tip clearances. Computations were performed for operating conditions from choke to stall and compared with measurements at the same conditions. Figure 9 shows calculated static pressure variation at a location on the rotor suction surface 36% axial chord downstream of the leading edge and 3 mm inboard of the blade

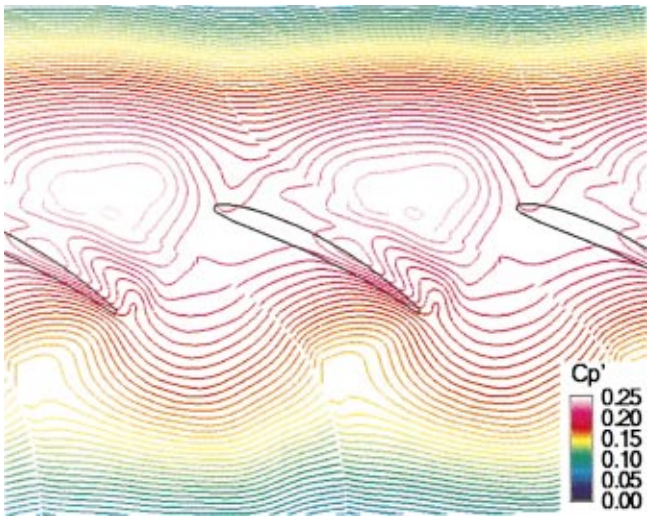

Fig. 10 Calculated standard deviation of pressure on casing

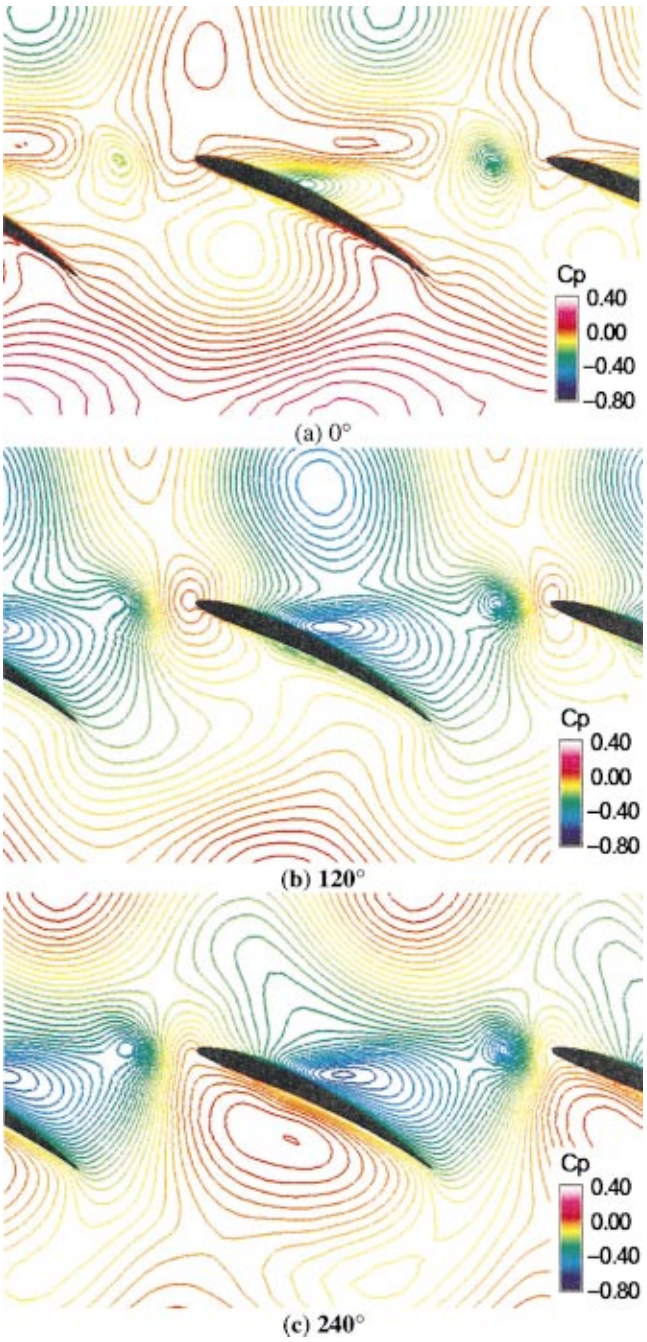

Fig. 11 Calculated instantaneous pressure field during one instability cycle

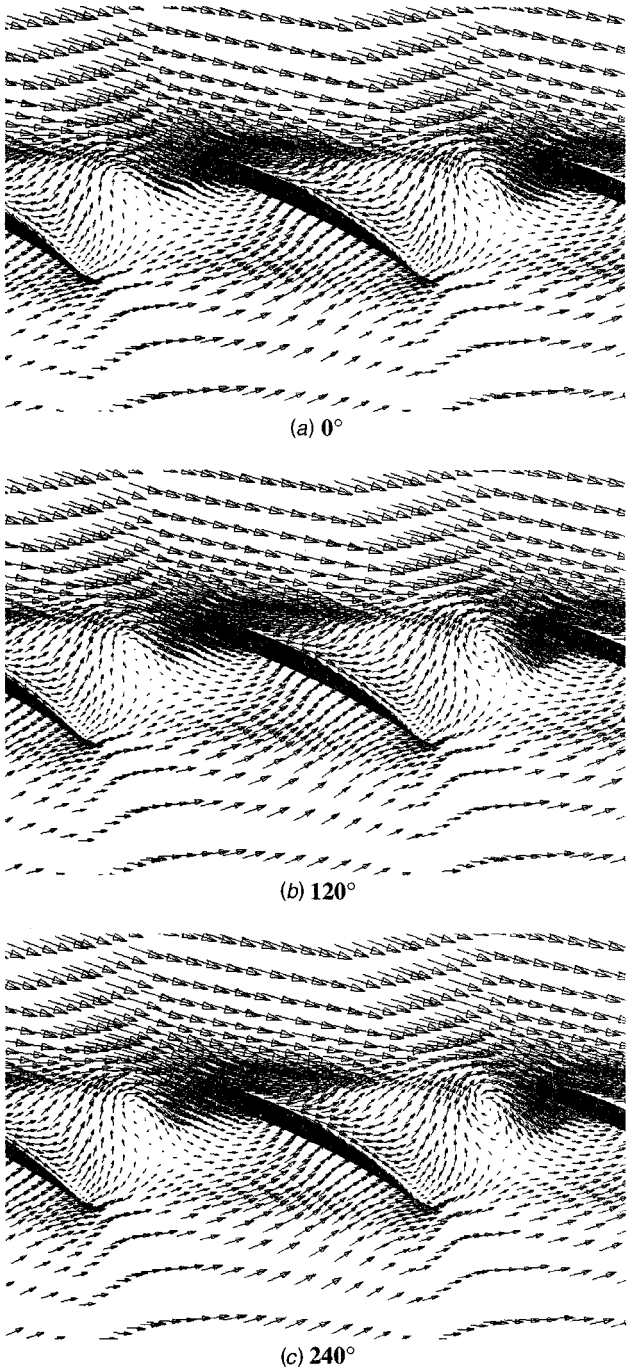

Fig. 12 Calculated instantaneous velocity vectors during one instability cycle

tip. The almost periodic variation in static pressure indicates the instability cycle. The measured pressure signal shown in Fig. 6 exhibits very similar behavior with more complex variation during each cycle.

Figure 10 shows the calculated distribution of the standard deviation of static pressure on the casing. The standard deviation was calculated from instantaneous flow solutions during one instability cycle. Passage-to-passage variations of the standard deviation were negligible in the numerical solution. The peak value of the calculated standard deviation is located further away from the pressure side of the blade and further upstream than that of the measurements in Fig. 5. This difference may be due to the relatively coarse computational grid and/or inadequacy of the currently applied turbulence model.

Figure 11 shows the calculated instantaneous static pressure distribution on the casing at three instants during one instability cycle. As seen in the measurements (Fig. 8), the calculation also shows a region of low static pressure moving from the suction side of the passage to the pressure side at roughly half the rotor speed.

To investigate the mechanism behind this observation, the calculated flow field was examined further. Figure 12 shows instantaneous velocity fields at the rotor tip at three instants during the instability cycle. Axially reversed flow extending over the entire circumferential direction is observed near the trailing edge. Calculated instantaneous streamlines are shown in Fig. 13. Both Figs. 12 and 13 show a vortex in the middle of the blade passage moving from the suction side of the passage to the pressure side at roughly half the rotor speed. The strength of the vortex varies

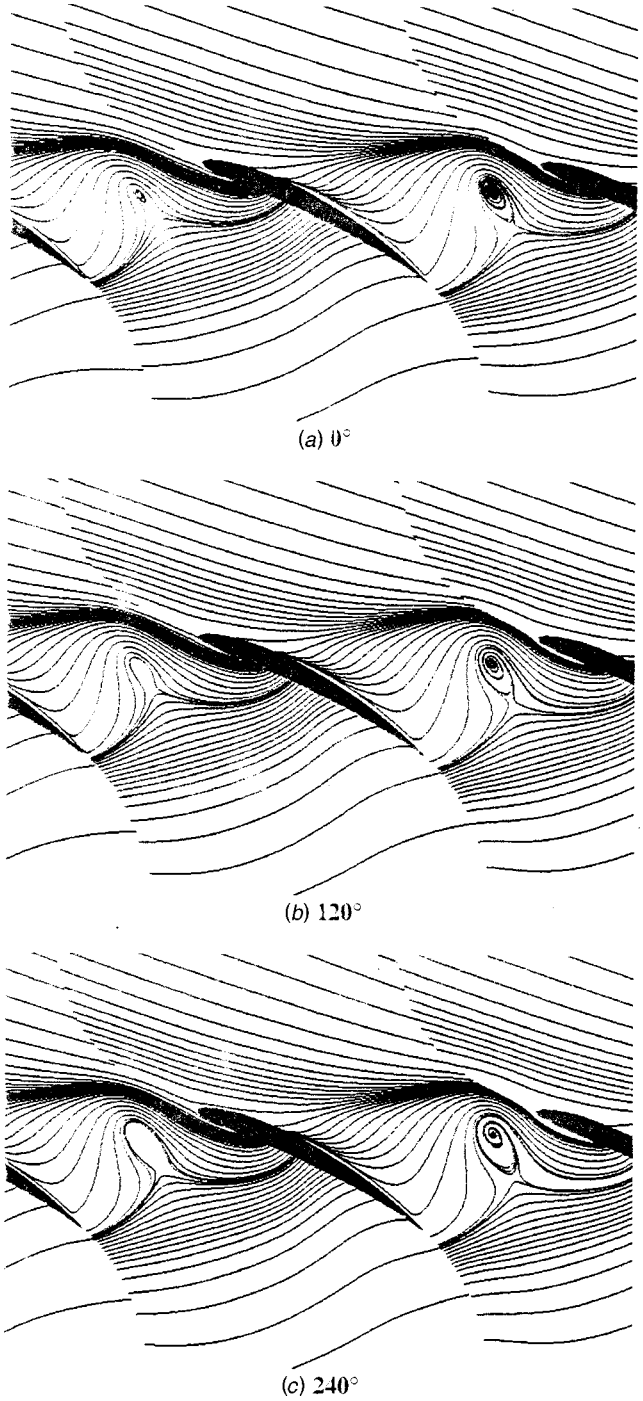

Fig. 13 Calculated instantaneous streamlines during one instability cycle

between different passages at different times. As this vortex moves in the tangential direction, the local pressure field also changes due to the change in blockage.

A three dimensional view of the vortex is shown in Fig. 14 with particle traces in an instantaneous three-dimensional flow field. This vortex, denoted as the rotating instability vortex in Fig. 14, seems to be different from the classical tip clearance vortex. Flow near the trailing edge is pushed forward by the axially reversed flow seen in Fig. 12. It then interacts with the tip clearance flow and the incoming flow and results in the rotating instability vortex. This vortex is formed periodically mid-way between the blades and moves toward the pressure side of the passage. Unsteady behavior of this vortex structure is the main mechanism of the rotating instability.

The calculated static pressure history near the blade tip in Fig. 9 shows periodic behavior. This is due to the movement of the rotating instability vortex shown in Fig. 14. The current numerical solution does not show clear periodic variation of flow properties across blade passages, as suggested by Mailach et al. [12]. Instead, the flow structure varies among blade passages in a rather random fashion. The number of instability cells can be determined either by circumferential mode analysis [1], or from frequencies in the relative and absolute frames (shown in Figs. 9 and 1, respectively) which was kindly suggested to the authors by Smith [13]. For the current operating condition, both methods indicate that there are about 30–35 cells, which is more than the number reported by Mailach et al. [12] for a different compressor. It seems that the number of instability cells depends on the specific design of the rotor and its operating condition.

Figure 15 shows a close-up of calculated velocity vectors inside the tip clearance near the rotating instability vortex and the blade leading edge. Previous studies (Smith [14], Koch [15]) have indicated that instability arises when the tip clearance flow spills into the adjacent blade passage from the pressure side at the leading edge. The results in Fig. 15 show that the tip clearance flow does not spill into the next blade passage at the leading edge. Instead, the flow follows the pressure side of the leading edge. The flow structure seen in Fig. 15 seems to be the reason why the compressor operates in a very stable mode even with the rotating instability.

Concluding Remarks

Summary. Experimental and numerical studies were conducted to understand the mechanisms of a rotating instability observed in a compressor operating near stall with a large tip clearance.

To detect the rotating instability, unsteady pressures were measured with high-resolution pressure transducers on the casing and near the blade tip. Ensemble-averaged plots of the casing pressures and their deviations suggest that the flow field becomes unsteady with large tip clearances. The measured data indicate that an intermittent low-pressure region traverses the blade passage near the tip. Therefore, two distinct trajectories of tip clearance flow exist near the casing: one that leaves the passage, and the other that impacts the following blade's pressure side.

A three-dimensional unsteady calculation was performed for the full annulus of the rotor to examine the nature of this flow structure and the rotating instability. The unsteady calculation captures the measured flow features well enough to explain the underlying physics of the flow field. With a large tip clearance, the blockage becomes very large near the casing, and axially reversed flow develops over the entire circumferential direction with a decrease in the flow rate. The tip clearance flow coming directly over the blade tip is pushed further upstream by the reversed endwall flow.

What We Learned. The present study shows that the tip clearance flow does not spill into the next blade passage when a rotating instability occurs; instead, the incoming flow follows the pressure side of the leading edge. Consequently, the tip clearance flow, the axially reversed flow near the casing, and the incoming flow interact near the leading edge and form a distinctive vortex structure. This vortex structure moves from the suction side of the passage to the pressure side at roughly half of the rotor speed. The vortex formation in the middle of the passage and its relative pitchwise movement are the main mechanisms of the rotating instability. The compressor operates in a very stable mode even when rotating instability is observed. This is because the tip clearance flow does not spill over into the following blade passage. If

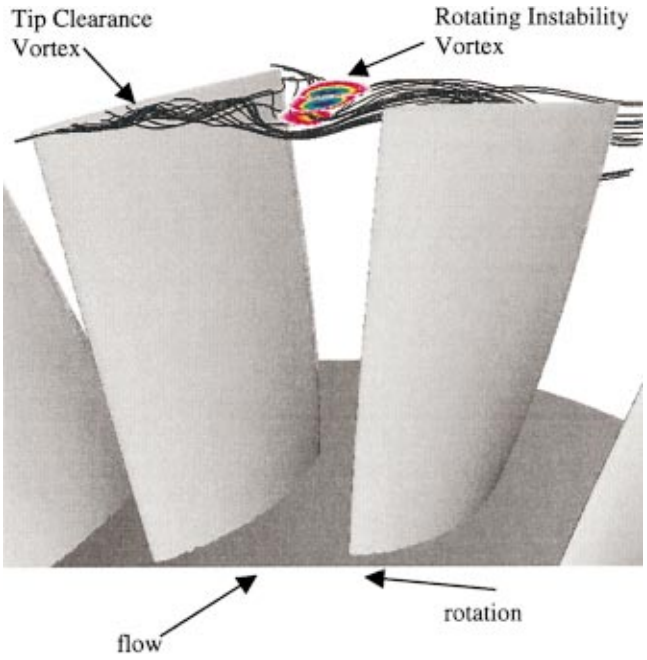

Fig. 14 Structure of instantaneous flow field

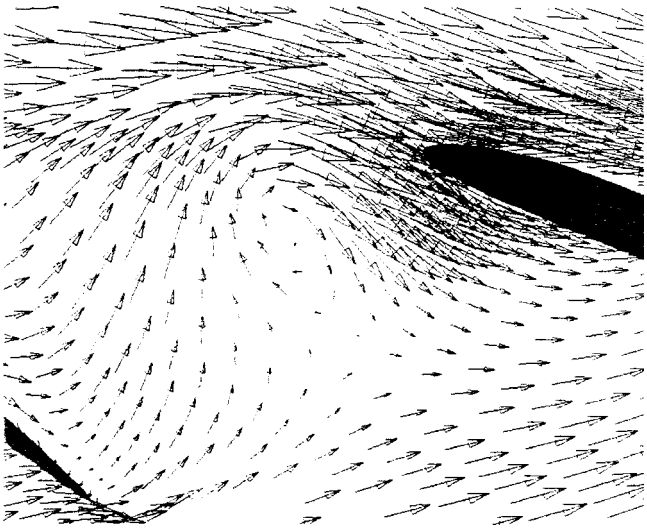

Fig. 15 Flow field near leading edge

the flow rate is further reduced and the in-passage vortex moves upstream of the leading edge, the tip clearance flow spills into the following blade passage and traditional rotating stall occurs.

Acknowledgments

The experimental part of this work was supported by the German Ministry for Research and Technology (BMBF) within the framework of AG Turbo Turbotech II (Teilprojekt 1.245, Förderkennzeichen 0327040D). The study was continued within ''Sonderforschungsbereich 557, Beeinflussung komplexer turbulenter Scherströmungen, TU Berlin'' of the German National Science Foundation. The authors would like to acknowledge the contribution of J. Loellbach of ICOMP during the course of the current study, and to thank Dr. L. H. Smith Jr. of G.E. Aircraft Engines for providing a method of calculating the number of instability cells with measured frequencies and helping to clarify related flow physics.

Nomenclature

n = rotor speed (1/min)
BPF = blade passing frequency
ϕ = flow rate
ψ = pressure coefficient
ζ = tip clearance, nondimensionalized by tip chord
C_P = static pressure coefficient, nondimensionalized by dynamic head of rotor tip speed
C'_P = static pressure fluctuation coefficient, nondimensionalized by tip stagnation pressure
μ = ensemble average of static pressure
p'_{rms} = standard deviation of pressure
i = index in axial direction
j = index in circumferential direction

References

[1] Kameier, F., and Neise, W., 1997, ''Experimental Study of Tip Clearance Losses and Noise in Axial Turbomachines and Their Reduction,'' ASME J. Turbomach., **119**, pp. 460–471.
[2] Liu, J.M., Holste, F., and Neise, W., 1996, ''On the Azimuthal Mode Structure of Rotating Blade Flow Instabilities in Axial Turbomachines,'' AIAA Pap., 96-1741, 2nd AIAA/CEAS Aeroacoustics Conference.
[3] März, J., Gui, X., Neuhaus, L., and Neise, W., ''Circumferential Structure of Rotating Instability Under Variation of Flow Rate and Solidity,'' VDI-Ber., **1425**, pp. 189–198.
[4] Baumgartner, M., Kameier, F., and Hormouziadis, J., 1995, ''Non Engine Order Blade Vibration in a High Speed Compressor,'' ISABE 95-7094, Twelfth Int. Symp. on Airbreathing Engines, Melbourne, Australia.
[5] Müller, R, and Mailach, R., 1998 ''Experimentelle Untersuchung von Verdichterinstabilitäten am Niedergeschwindigkeitsverdichter Dresden,'' VDI-Berichte 1425, pp. 167-176, VDI-GET-Tagung Turbokompressoren im industriellen Einsatz, Hannover, Germany.
[6] Hah, C., 1984, ''A Navier-Stokes Analysis of Three-Dimensional Turbine Flows Inside Turbine Blade Rows at Design and Off-Design Conditions,'' ASME J. Eng. Gas Turbines Power, **106**, pp. 421–429.
[7] Hah, C., 1987, ''Calculation of Three-Dimensional Viscous Flows in Turbomachinery with an Implicit Relaxation Method,'' AIAA J. Propul. Power, **3**, No. 5, pp. 415–422.
[8] Cho, N.-H., Liu, X., Rodi, W., and Schonung, B., 1992, ''Calculation of Wake-Induced Unsteady Flow in a Turbine Cascade,'' ASME Paper 92-GT-306.
[9] Hah, C., Puterbaugh, S.L., and Copenhaver, W.W., 1993, ''Unsteady Aerodynamic Phenomena in a Transonic Compressor Stage,'' AIAA Pap., 93-1868.
[10] Hah, C., Schulze, R., Wagner, S., and Hennecke, D. K., 1999, ''Numerical and Experimental Study for the Short Wavelength Stall Inception in a Low-Speed Axial Compressor,'' Proc. Fourteenth ISABE Conference, IS-234.
[11] Zierke, W.C., Farrell, K.J., and Straka, W.A., 1994, ''Measurements of Tip Clearance Flow for a High Reynolds Number Axial-Flow Rotor: Part 1—Flow Visualization,'' ASME Paper 94-GT-453.
[12] Mailach, R., Lehmann, I., and Vogeler, K., 2000, ''Rotating Instabilities in an Axial Compressor Originating from the Fluctuating Blade Tip Vortex,'' ASME Paper 2000-GT-506.
[13] Smith, L. H., 2001, private communication.
[14] Smith, L.H., 1970, ''Casing Boundary Layers in Multistage Axial-Flow Compressors,'' *Flow Research and Blading*, Elsevier, Amsterdam The Netherlands.
[15] Koch, C. C., 1981, ''Stalling Pressure Rise Capability of Axial Compressor Stage,'' ASME J. Eng. Power, **98**, pp. 411–424.

Discussion: "An Experimental and Numerical Invesitgation Into the Mechanism of Rotating Instability" (Maerz, J., Hah, C., and Neise, W., 2002, ASME J. Turbomachinery, 124)

Nick Cumpsty
Rolls-Royce plc.
e-mail: nick.cumpsty@rolls-royce.com

There is a lot to admire in this paper and I congratulate the authors in using experiment and CFD to contribute to the understanding of a complicated phenomenon. Once a flow becomes

nonuniform, as it does for the flow described here, there are many more degrees of freedom and the flow can establish itself in many different ways. In consequence, flow that is stalled (in the sense that this takes for rotating stall in compressors) can exhibit many different arrangements. I would like to suggest that the rotating disturbance found here is a particular type of rotating stall corresponding to the special circumstances of an isolated rotor with large tip clearance.

The problem that I have with this paper and with others that have come from Germany over the last few years is the term ''rotating instability.'' One of the useful conclusions from the present paper, referred to in the section ''What We Learned,'' is that the flow is actually very stable. In fact, a condition of instability is very hard to observe, since it is by its very nature transient: A pencil standing vertically on its point is in a condition of instability, but the moment it is microscopically perturbed it ceases to be in the state of instability but is falling toward its new stable condition. The compressor will similarly be unstable at the instant before it moves from being unstalled to being in rotating stall; similarly, for a compressor in rotating stall, there will be an instantaneous condition of instability as the throttle is opened and it moves from stalled to unstalled. The stalled condition, however, is normally very stable.

I have been told that the term ''rotating instability'' is well established and it is implied by this that it should remain in circulation. The term gained currency in Germany a few years ago to describe the type of rotating disturbance described in this paper. It was an unfortunate choice then and remains unfortunate now. It is a widely recognized feature of the English language that words can be created, adapted, and re-used to suit needs. One of the most famous of English quotations is ''What's in a name? that which we call a rose by any other name would smell as sweet'' (*Romeo and Juliet*: Shakespeare). While accepting the spirit of this quotation, it is also true that it would be confusing to refer to a rose using the word ''thorn,'' or even the word ''garlic.'' Put another way, if we want to choose a new use for a word, we should make sure that it does not have a prior meaning that could be confusing, by implying properties that do not apply. Such is the case for ''rotating instability,'' which strictly has no clear meaning, but which implies a special condition that is inconsistent with the stable behavior of the rotating stall flow pattern that is the subject of this paper.

Closure to ''Discussion of 'An Experimental and Numerical Investigation into the Mechanisms of Rotating Instability' '' (2002, ASME J. Turbomach., 124)

J. Maerz

C. Hah
e-mail: chunhill.hah@aki.lerc.nasa.gov

W. Neise

NASA Glenn Research Center, 21000 Brookpark Rd., Cleveland, OH 44135

The authors would like to thank Prof. Cumpsty for sharing his insight and his view of the flow phenomena we investigated.

We agree that the stage's overall behavior in rotating instability is indeed stable. This implies that the observed phenomenon, rather than being of transient nature, exhibits constant statistical properties (frequencies, amplitudes, etc.). On a smaller scale, looking at the flow in an individual blade passage, complex three-dimensional events take place periodically which this paper aims to identify.

The fact that the overall performance of the turbomachine is stable does not contradict the existence of flow instabilities in certain regimes, as is the case in a free jet flow which is fully stable globally, but undisputedly exhibits flow instabilities in the intrinsic flow of the free shear layer.

In earlier work, the first proposed cause of the observed behavior was periodic flow separation. Looking at the simplified example of 2-D flow around an airfoil, separation certainly fulfills the requirements of flow instability: the flow departs into a different state with a recirculation region.

In the case of rotating stall, the blades communicate their stalled state by inducing a different angle of attack on neighboring blades. If turbomachines were not round one might call this ''propagating stall,'' and having identified individual blade stall as a flow instability, we might as well call it, more generally, ''propagating flow instability.'' Is it, in the absence of further knowledge, inadequate to generalize an unknown propagating disturbance of the local tip flow as ''rotating instability''?

Thus, we assume that on a blade-pitch scale we are dealing with a flow instability that is triggered/phase locked by its neighboring blades into a periodic pattern (which must satisfy the condition of 2π-periodicity), and therefore becomes regular. The phase-locked phenomenon, on a global (stage) scale, exhibits steady periodic behavior.

Not knowing the detailed flow pattern, the term rotating/propagating flow instability is therefore the more cautious term, as we do not positively know that the flow really ''stalls'' in the tip region (though a recirculation region of some kind almost certainly occurs). There is more evidence that ''rotating instability'' and ''rotating stall'' are different, though related, phenomena: the number of ''cells'' involved in rotating instability is larger by an order of magnitude than in the case of rotating stall. We have observed rotating instability alone near design point operation, rotating instability plus rotating stall simultaneously when approaching the stall line, and, of course, rotating stall alone when the machine is throttled further.

Incidentally, the term ''rotating instability'' was not coined in Germany: Bent et al.[1] investigated the generation of broadband noise in centrifugal pump impellers and called the observed disturbance of the discharge flow ''rotating stall-like instability'' as well as a ''rotating flow instability.''

The authors agree with Prof. Cumpsty that perhaps the phenomena could be described with a different term (like ''rotating tip vortex instability'' or ''rotating tip vortex disturbance''). However, the term ''rotating instability'' has been used to describe the phenomenon in earlier studies, in consideration of particular features of the flow. We, therefore, used the same terminology to identify the flow phenomenon in our paper.

[1]Bent, McLaughlin, Thompson: ''The Influence of Discharge Configuration on the Generation of Broadband Noise in Centrifugal Turbomachinery.'' DGLR/AIAA Aeroacoustics Conference 1992, 92-02-099.

